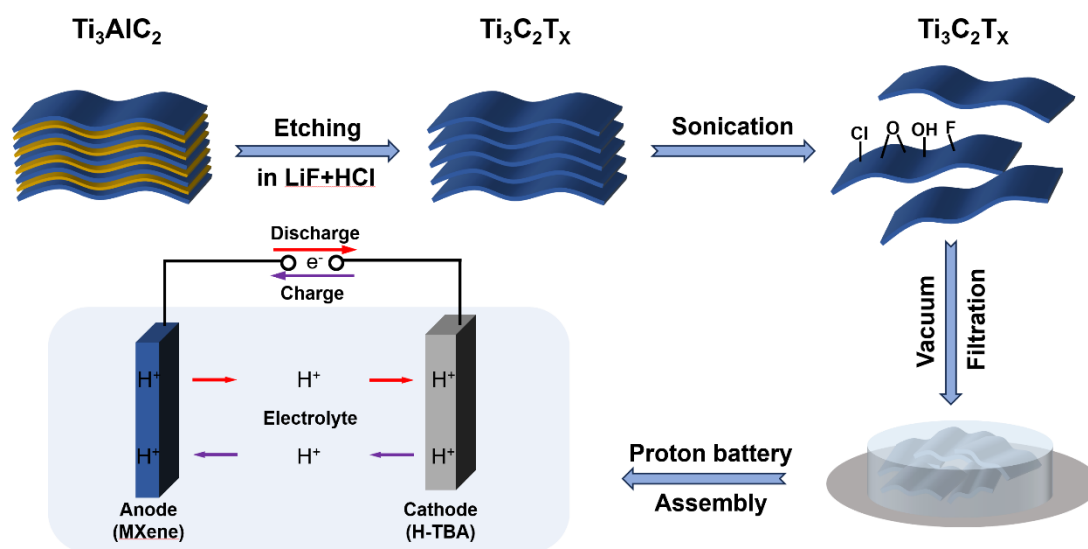


Supplementary Information



Scheme S1 Synthesis scheme of the vacuum-filtered $\text{Ti}_3\text{C}_2\text{T}_x$ film electrode and assembly schematic of the proton battery.

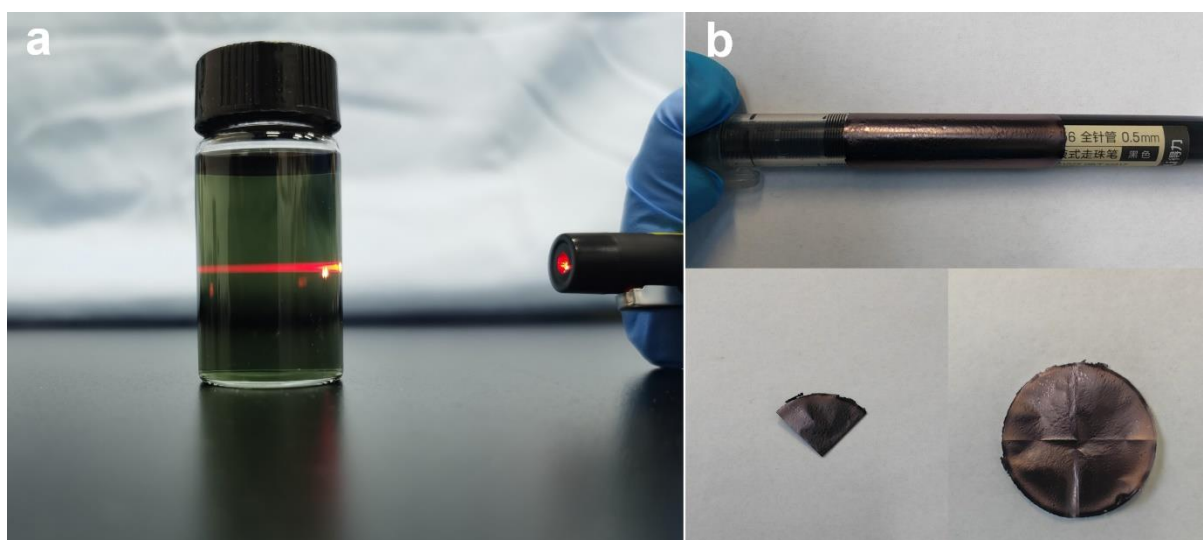


Figure S1 (a) Dingdall phenomenon of diluted few-layer $\text{Ti}_3\text{C}_2\text{T}_x$ colloidal solution. (b) Optical image of the vacuum-filtered $\text{Ti}_3\text{C}_2\text{T}_x$ MXene film. The film exhibits excellent flexibility.

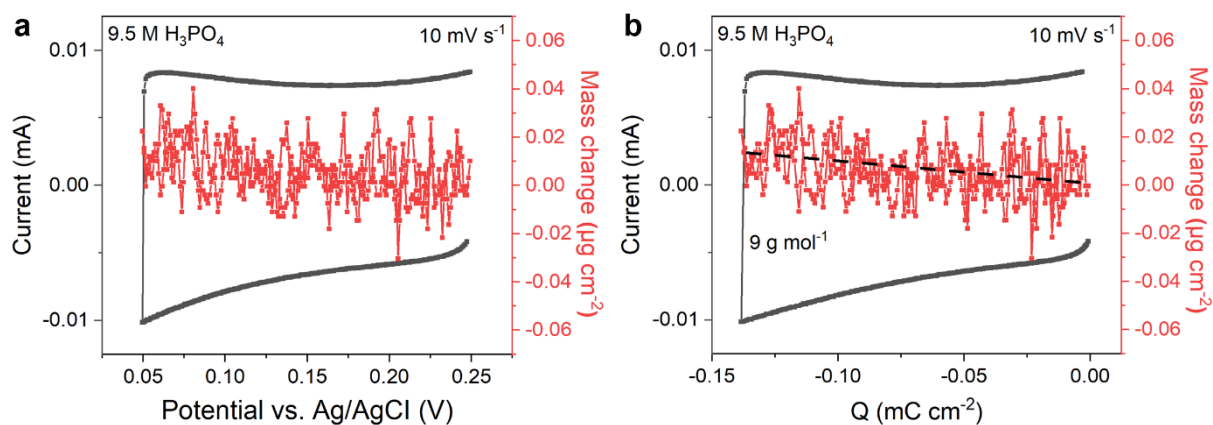


Figure S2 (a) CV profile and electrode mass response and (b) electrode mass change versus charge for $\text{Ti}_3\text{C}_2\text{T}_x$ MXene on an Au-coated quartz crystals substrate recorded at 10 mV s^{-1} with a potential range of 0.05 to 0.25 V in 9.5 M H_3PO_4 .

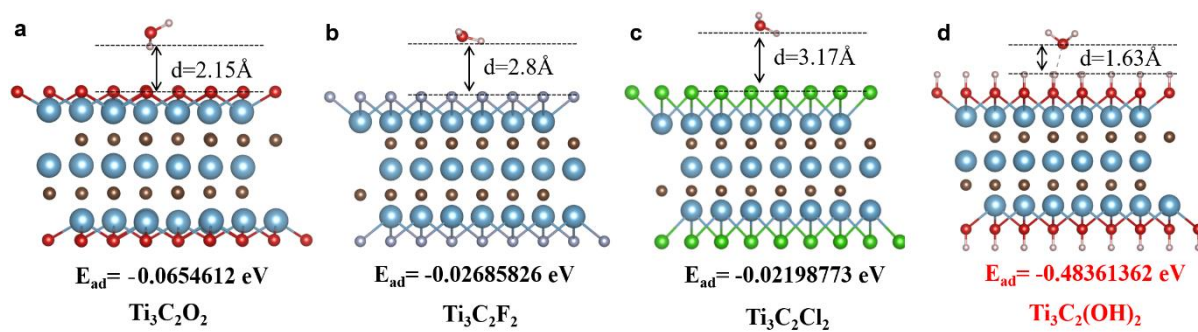


Figure S3 Adsorption energy of H_2O on the surface of (a) $\text{Ti}_3\text{C}_2\text{O}_2$, (b) $\text{Ti}_3\text{C}_2\text{F}_2$, (c) $\text{Ti}_3\text{C}_2\text{Cl}_2$, and (d) $\text{Ti}_3\text{C}_2(\text{OH})_2$.

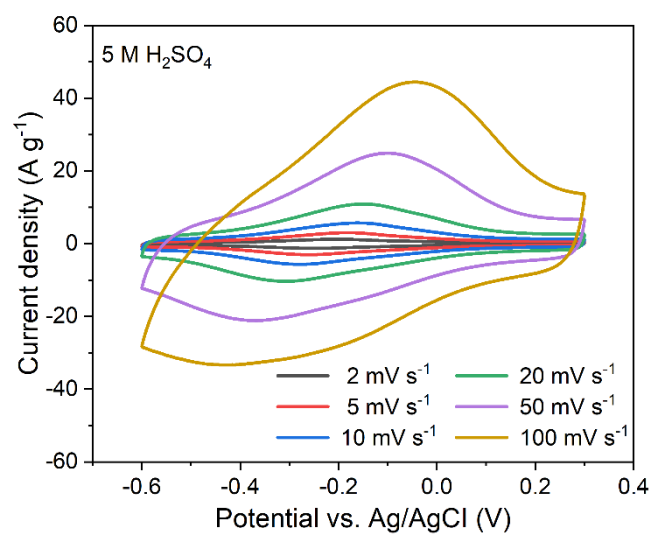


Figure S4 Cyclic voltammograms of the $\text{Ti}_3\text{C}_2\text{T}_x$ MXene film electrode measured at different scan rates in $5\text{ M H}_2\text{SO}_4$.

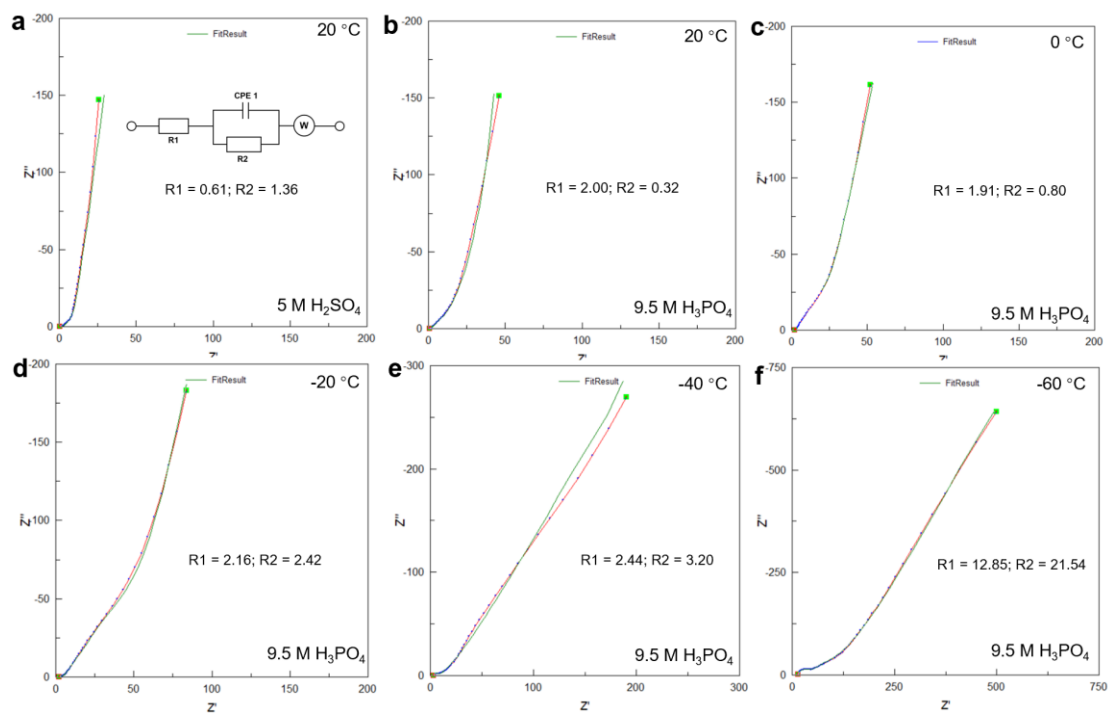


Figure S5 Fitted EIS plots shown in Figure 4d and 4e using Zview software.

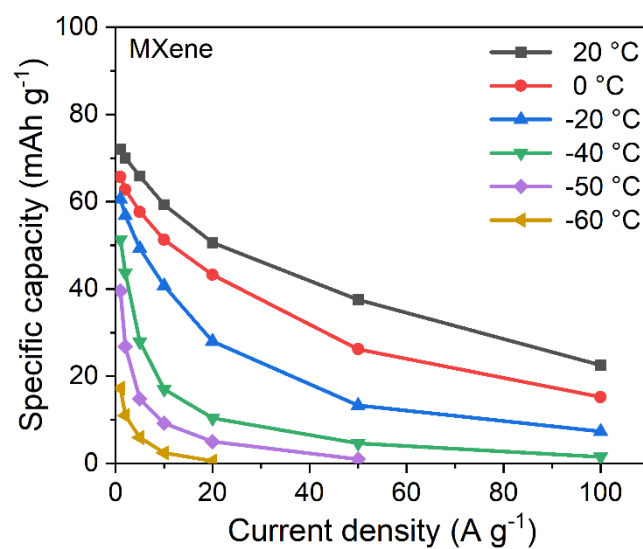


Figure S6 Specific gravimetric capacity vs. current density for $\text{Ti}_3\text{C}_2\text{T}_x$ MXene film electrode measured at different temperatures in 9.5 M H_3PO_4 .

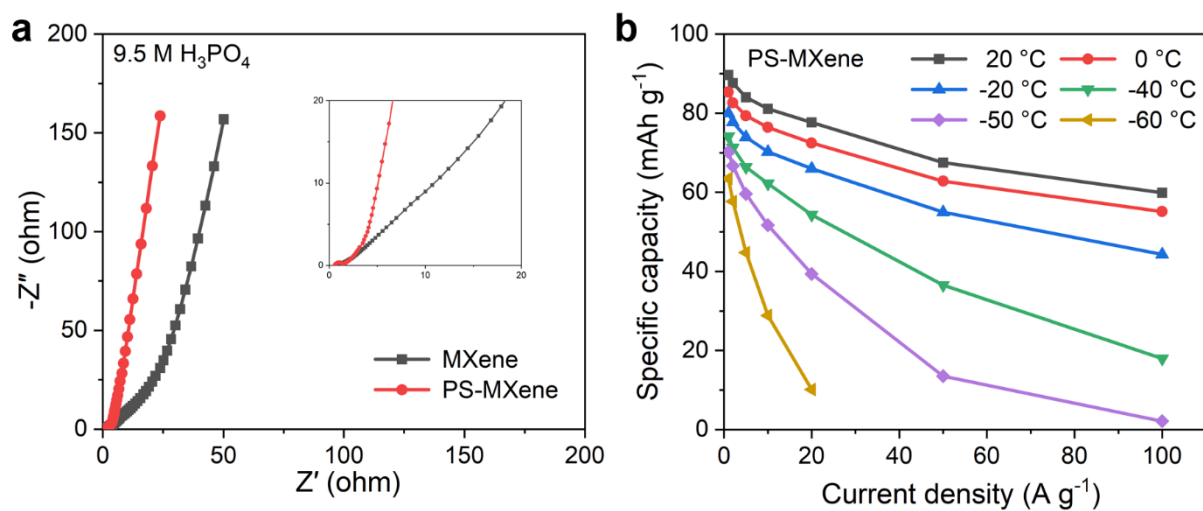


Figure S7 (a) Electrochemical impedance spectroscopy of the $Ti_3C_2T_x$ MXene and PS-MXene film electrodes collected at 0.2 V *vs.* Ag/AgCl in 9.5 M H_3PO_4 . The inset shows the high-frequency range. (b) Specific gravimetric capacity *vs.* current density for PS-MXene film electrode at different temperatures.

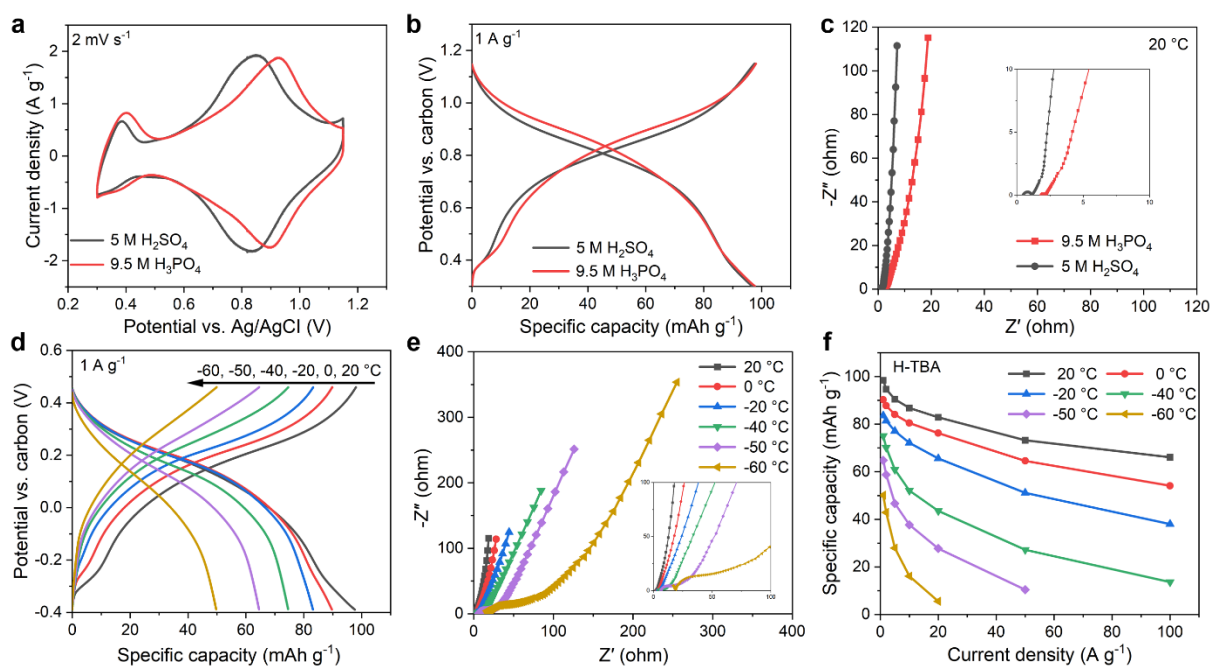


Figure S8 Electrochemical performance of H-TBA in acid electrolyte. (a) Cyclic voltammograms of H-TBA at a scan rate of 2 mV s⁻¹ in 5 M H₂SO₄ and 9.5 M H₃PO₄, respectively. (b) Galvanostatic charge-discharge profiles of H-TBA at a current density of 1 A g⁻¹ in 5 M H₂SO₄ and 9.5 M H₃PO₄. (c) Electrochemical impedance spectroscopy of H-TBA collected at 0.8 V vs. Ag/AgCl in 5 M H₂SO₄ and 9.5 M H₃PO₄. The inset shows the high-frequency range. (d) Galvanostatic cycling profiles of H-TBA at different temperatures with current density of 1 A g⁻¹ in 9.5 M H₃PO₄. (e) Electrochemical impedance spectroscopy data of H-TBA collected at 0.1 V vs. carbon at different temperatures in 9.5 M H₃PO₄. The inset shows the high-frequency range. (f) Specific gravimetric capacity vs. current density for H-TBA at different temperatures.

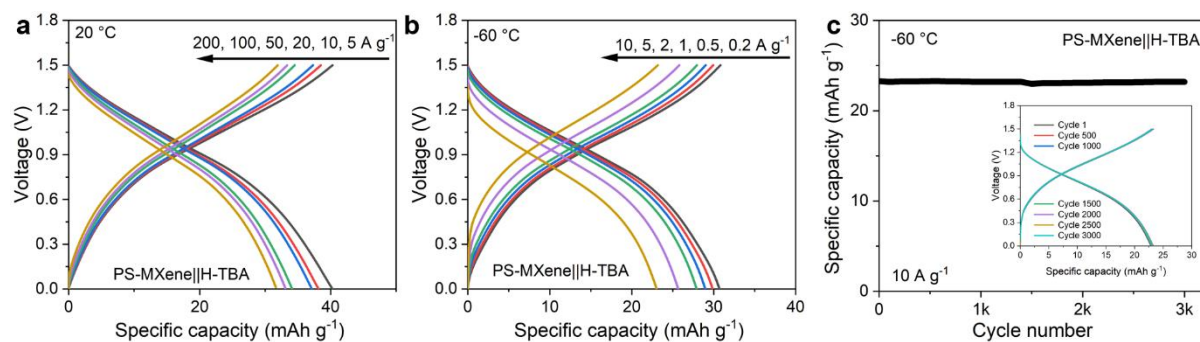


Figure S9 Electrochemical performance of PS-MXene||H-TBA proton battery in 9.5 M

H_3PO_4 . (a) Galvanostatic charge-discharge profiles of proton battery measured at 20 °C with

(a) current densities of 5, 10, 20, 50, 100, 200 A g^{-1} and (b) -60 °C with current densities of

0.2, 0.5, 2, 5, 10 A g^{-1} . (c) Capacity retention of PS-MXene||H-TBA proton battery at -60 °C.

The inset shows galvanostatic cycling data collected at 10 A g^{-1} .

Table S1 Comparison of some previous studies that used acidic electrolyte

Anode	Cathode	Electrolyte	Temp.	Capacity	Cycling at room T
Ti ₃ C ₂ T _x ^[S1]	AC	5 M H ₂ SO ₄	-50°C	88 mAh g ⁻¹ at -50°C, 104 mAh g ⁻¹ at 20°C	78% capacity retention after 20,000 cycles
MoO ₃ ^[S2]	APB	9.5 M H ₃ PO ₄	-78°C	180 mAh g ⁻¹ at -40°C, 220 mAh g ⁻¹ at 20°C	~85% capacity retention after 200 cycles
MoO ₃ ^[S3]	MnO ₂	2 M H ₂ SO ₄ +2 M MnSO ₄	-70°C	170.8 mAh g ⁻¹ at -70°C, 210.7 mAh g ⁻¹ at 20°C	81% capacity retention after 300 cycles
PTO ^[S4]	MnO ₂	2 M H ₂ SO ₄ +2 M MnSO ₄	-70°C	105 mAh g ⁻¹ at -70°C, 150 mAh g ⁻¹ at 20°C	80% capacity retention after 5,000 cycles
Ti ₃ C ₂ T _x (This work)	H-TBA	9.5 M H ₃ PO ₄	-60°C	64 mAh g ⁻¹ at -60°C, 90 mAh g ⁻¹ at 20°C	No capacity fading after 25,000 cycles

References

- [S1] J. Xu, X. Hu, X. Wang, X. Wang, Y. Ju, S. Ge, X. Lu, J. Ding, N. Yuan, Y. Gogotsi, Low-temperature pseudocapacitive energy storage in Ti₃C₂T_x MXene. *Energy Storage Mater.* **33**, 382–389 (2020).
- [S2] H. Jiang, W. Shin, L. Ma, J. J. Hong, Z. Wei, Y. Liu, S. Zhang, X. Wu, Y. Xu, Q. Guo, M. A. Subramanian, W. F. Stickle, T. Wu, J. Lu, X. Ji, A high-rate aqueous proton battery delivering power below -78 °C via an unfrozen phosphoric acid. *Adv. Energy Mater.* **10**, 2000968 (2020).
- [S3] L. Yan, J. Huang, Z. Guo, X. Dong, Z. Wang, Y. Wang, Solid-State Proton Battery Operated at Ultralow Temperature. *ACS Energy Lett.* **5**, 685-691 (2020).
- [S4] Z. Guo, J. Huang, X. Dong, Y. Xia, L. Yan, Z. Wang, Y. Wang, An organic/inorganic electrode-based hydronium-ion battery. *Nat. Commun.* **11**, 959 (2020).